promoting access to White Rose research papers

Universities of Leeds, Sheffield and York
http://eprints.whiterose.ac.uk/

This is an author produced version of a paper published in **Journal of Applied Physics**.

White Rose Research Online URL for this paper:
http://eprints.whiterose.ac.uk/74868

Published paper

Dawson, J.A., Harding, J.H., Chen, H.R., Sinclair, D.C. (2012) *First principles study of intrinsic point defects in hexagonal barium titanate*, Journal of Applied Physics, 111 (9), Article number 094108
http://dx.doi.org/10.1063/1.4711099

White Rose Research Online
eprints@whiterose.ac.uk

First-principles study of intrinsic point defects in hexagonal barium titanate

J. A. Dawson, J. H. Harding, H.-R. Chen and D. C. Sinclair

Department of Materials Science and Engineering, University of Sheffield, Sir Robert Hadfield Building, Mappin Street, Sheffield, S1 3JD, UK

Density functional theory (DFT) calculations have been used to study the nature of intrinsic defects in the hexagonal polymorph of barium titanate. Defect formation energies are derived for multiple charge states and due consideration is given to finite-size effects (elastic and electrostatic) and the band gap error in defective cells. Correct treatment of the chemical potential of atomic oxygen means that it is possible to circumvent the usual errors associated with the inaccuracy of DFT calculations on the oxygen dimer. Results confirm that both mono- and di-vacancies exist in their nominal charge states over the majority of the band gap. Oxygen vacancies are found to dominate the system in metal-rich conditions with face sharing oxygen vacancies being preferred over corner sharing oxygen vacancies. In oxygen-rich conditions, the dominant vacancy found depends on the Fermi level. Binding energies also show the preference for metal-oxygen di-vacancy formation. Calculated equilibrium concentrations of vacancies in the system are presented for numerous temperatures. Comparisons are drawn with the cubic polymorph as well as with previous potential-based simulations and experimental results.

[a)]Electronic mail: mtp09jd@sheffield.ac.uk

I. INTRODUCTION

The perovskite, barium titanate, receives considerable attention for its electrical properties which include ferroelectricity, piezoelectricity and a high dielectric constant[1-3]. Such properties mean that it plays a major role in numerous technological applications including multi-layer capacitors and positive temperature coefficient (PTC) thermistors. It is not only the cubic close packed perovskite structure (*c*-$BaTiO_3$) that displays useful properties; the high temperature (> 1425 ˚C) hexagonal polymorph (*h*-$BaTiO_3$) also displays interesting and potentially useful electrical properties depending upon the temperature[4-6] and chemical dopants present[7]. In addition to these electrical properties, semiconductivity can also be induced in undoped *h*-$BaTiO_3$ as a result of partial reduction of Ti^{4+} to Ti^{3+} ions when samples are prepared at high temperature under inert or reducing conditions[8,9]. Through partial re-oxidation of these samples, 'colossal' permittivity effects can be achieved[8]. Samples prepared in this way also result in oxygen deficiency; both experiment and simulation have confirmed that the oxygen loss occurs solely at face sharing (O1) sites[9-11], see Fig. 1(a). Such intrinsic defects are crucial in controlling the electrical properties in this semiconducting material as illustrated by recent publications by Natsui *et al*[12,13] on the diffusion behaviour of oxygen in *h*-$BaTiO_3$. As is the case with the other polymorphs of $BaTiO_3$, the main focus of research on *h*-$BaTiO_3$ is on doping and in particular, on transition metal doping[14,15].

While there exists a significant number of DFT studies completed on *c*-$BaTiO_3$[16-19], there are very few DFT studies (or indeed simulation studies) on the hexagonal polymorph. Colson *et al*[11], however, did complete calculations on both the *c*- and *h*-polymorphs and obtained good agreement with experimental structures as well as simulating Ru-doping of the *h*-polymorph at multiple concentrations. Furthermore, defect formation energies have been derived for intrinsic

mono- and di-vacancies using DFT for *c*-$BaTiO_3$[17], although unlike in this work, the oxygen chemical potential was established by calculating the total energy of the oxygen dimer directly, whereas ideal gas relations were used for our calculations of the oxygen chemical potential (see Sec. II B). To the best of our knowledge no other in-depth study of intrinsic defect thermodynamics in *h*-$BaTiO_3$ exists.

In this work, the Zhang-Northrup formalism[20] is used to establish defect formation energies. In this formalism, the defect formation energy is defined as the difference between the Gibbs free energies of the defective and perfect cell with regard to specific chemical potentials and the contribution of electrons being added and removed. One drawback of zero-temperature DFT calculations is the exclusion of entropic and pressure/volume contributions to the Gibbs free energy of each particle. While this is a minor factor for solids as these contributions are small, it does present a significant issue for calculations on gaseous particles where such contributions are much larger. This problem can be corrected through the use of ideal gas physics in a method described by Finnis *et al*[21] and employed more recently for the calculation of defect formation energies for alumina[22]. Through the use of this method, chemical potentials for atomic species, namely oxygen in our case, can be made more accurate thorugh the combination of DFT calculations and standard thermodynamics as well as being defined for a specific temperature and oxygen partial pressure. The Gibbs free energy of a solid can be accurately determined by using the ground-state total energy obtained from DFT calculations.

The main purpose of this work is to determine accurate formation energies for the native defects of *h*-$BaTiO_3$. In addition to Ba (V_{Ba}), Ti (V_{Ti}) and O (V_O) mono-vacancies, Ti-O (V_{Ti} - V_O) and Ba-O (V_{Ba} - V_O) di-vacancies have also been considered, including the binding energies of such di-vacancies. Finite-size scaling and band gap corrections have also been applied. The

results show a large difference in energy between these defects and this is reflected in the calculated concentrations of each vacancy type and possible vacancy site. Such results will enable quantitative comparison both with experiment and with previous results calculated for *c*-$BaTiO_3$[17].

In the following section, we describe the computational approach and methods used to derive the formation energies and concentrations of the defects as well as the corrections involved. In Sec. III, the results are presented, including defect formation energies for all possible mono-vacancies and selected di-vacancies, binding energies of V_{Ti} - V_O and V_{Ba} - V_O defect pairs, cation vacancy concentrations and the relaxed defect geometries of the most prominent mono-vacancies. The work is concluded in Sec. IV.

II. METHODOLOGY

A. Computational details

All calculations in this work were performed using the Vienna *Ab initio* simulation package (VASP)[23] with the local density approximation (LDA)[24,25] and projector augmented-wave method[26.27]. The LDA was chosen to provide consistency with results previously obtained for the cubic polymorph of $BaTiO_3$[17]. For greater accuracy, the 3*s* and 3*p* electrons of the Ti atoms were included in the valence electrons for all calculations. Defect formation energies were calculated using the *h*-$BaTiO_3$ 30 atom unit cell as well as 60 (2 X 1 X 1) and 120 (2 X 2 X 1) atom supercells. A full description of the finite-size extrapolation procedure is given in Sec. II C. A **Γ**-point centred 4 X 4 X 3 *k*-point mesh was used for Brillouin zone integration for the 30 and 60 atom cells and a 3 X 3 X 2 mesh for the 120 atom cells. A plane wave cutoff energy of 500 eV

was applied for all defect calculations. In the case of charged defects, a neutralizing background charge was used to preserve cell neutrality.

B. Defect calculations

Using the Zhang-Northrup formalism[20], the formation energy ( ) of a defect in charge state can be calculated with respect to chemical potentials and the Fermi level: -

(1)

where is the total energy of the defective system and is the total energy of the perfect reference cell. The dependence upon the Fermi level, , is given in the second term, here is the position of the valence band maximum (VBM). In this equation, takes a value between 0 and E_g, where E_g is the band gap of the material. The final term defines the contribution of the chemical potentials of each atomic species, is the number of atoms of element *i* removed or added to create the defect, represents the chemical potential of element *i* and is the sum of the chemical potentials of the reference state and the chosen chemical environment (as calculated by equations 3-6 below). The chemical potential of the reference state for an element is equivalent to its calculated total free energy per atom (see Sec. III A).

From the calculation of defect formation energies, the concentration of that defect in equilibrium at a particular temperature can be obtained[28]: -

(2)

where is the concentration of possible defect sites, is the Boltzmann constant and T is the temperature. These values can enable quantitative comparison with experiment and in the case of h-$BaTiO_3$ an insight into preferred vacancy sites is provided.

For defect formation energy calculations, chemical potentials must be calculated to establish the thermodynamic boundaries of the system. As discussed in Sec. I, the small temperature and pressure dependence of the chemical potential per unit cell of a solid (e.g. Ba, Ti) can be neglected. This allows the use of T = 0 K total energy calculations for these atomic species and the bulk crystal (as well as its formation energy) to define thermodynamic reservoirs where the chemical potentials of the individual atoms cannot exceed the formation energy of the crystal: -

(3)

In addition to this condition, further constraints come from the formation of competing compounds: -

(4)

(5)

The combination of these equations confines the values of the chemical potentials of the atomic species to the stability range of $BaTiO_3$.

While it is acceptable to use T = 0 K total energy calculations to define thermodynamic boundaries for solids, the chemical potential of gaseous oxygen has a far stronger dependence upon temperature and pressure. Furthermore, the choice of functional and pseudopotentials in calculating results in significant error due to the inaccuracies of DFT in simulating the oxygen dimer as discussed by Hine *et al*[22]. In this work, a method developed by Finnis *et al*[21] is

used to avoid calculating directly from DFT calculations. By using the experimental formation energy of $BaTiO_3$ and T = 0 K total energy calculations for Ba and Ti, the oxygen chemical potential at standard pressure and temperature, , can be determined without the need for direct calculation. Through the use of ideal gas relations and , the oxygen chemical potential can be derived for a specific temperature and pressure, . The reliability of this approach has been confirmed by comparison to thermodynamic data[29]. The value of for a specific temperature and pressure is obtained from the ideal gas expression and formula for an ideal gas of rigid dumbbells: -

– – — (6)

The temperature contribution is represented by: -

– – — (7)

where is the molecular entropy of oxygen gas (0.0021 eV/K) and is its constant pressure heat capacity (7 /2); both values are taken from Ref. 30.

For most of the results reported here, a temperature of 1698 K and an oxygen partial pressure of 1 atm have been used to calculate in accordance with the experimental polymorphic phase transition conditions of *c*- to *h*-$BaTiO_3$.

C. Finite-size corrections

One disadvantage of these types of DFT calculation is the spurious defect-defect interactions that occur between periodic images, with the magnitude being very much dependent on the charge of the defect and the size and shape of the supercell[31,32]. Elastic interactions are the main source of error for neutral defects. These interactions scale inversely to supercell volume, L^{-3}, and hence are dealt with inherently by the finite-size scaling extrapolation process. For charged defects, electrostatic interactions can be corrected by a multipole expansion as presented by Makov and Payne[33]. The first term in this expression concerns monopole-monopole interactions and scales as L^{-1}. This correction can be determined with prior knowledge of the static dielectric constant of the crystal, ε, and the Madelung constant of the supercell, α,:-

(8)

Using first-principles calculations a value of $\varepsilon = 57$ was obtained for barium titanate[34], this value was used in the present work. The next term in the multipole expansion relates to monopole-dipole interactions. Similarly to the elastic interactions, this scales with L^{-3} and can therefore also be accounted for by the finite-size scaling procedure. The results of this procedure generally produced small extrapolation errors, as shown by Table 1. For strongly charged defects such Ti vacancies, quadrupole and higher terms may become important. However, they have not been considered in this work.

D. Band gap corrections

Another shortcoming of DFT calculations is the underestimation of the band gap[35]. To account for this problem, we use the same approach that was used by Erhart and Albe[17] for *c*-$BaTiO_3$. This method shifts the valence band ( ) and the conduction band ( ) with respect to each other so that the correction energy is obtained from: -

(9)

where and represent the number of electrons occupying conduction band states and the number of holes occupying valence band states, respectively. A T = 0 K a band gap of 3.4 eV derived from extrapolation of higher temperature data[36] was used to correct for the underestimation of the band gap while assuming the offset of the calculated band structure is restricted to the conduction band i.e. = 0 and = 3.4 eV - . Such corrections only affect oxygen vacancies and di-vacancies in charge states below their full ionic values i.e. , and . Furthermore, these defects already have significantly higher formation energies than the equivalent defect in its nominal charge state over the majority of the band gap (See Sec. III B) and the band gap corrections succeed in only further increasing these defect formation energies.

III. RESULTS AND DISCUSSION

A. Bulk properties

To define thermodynamic boundaries (as described in Sec. II B) the bulk properties of *h*-$BaTiO_3$ and its constituent elements/compounds in their standard states must be calculated. All

bulk property calculations were completed using a Γ-point centred 13 X 13 X 13 *k*-point mesh and were fully converged to an accuracy greater than 1 meV per unit cell.

A lattice constant of 4.77 Å and a total energy of -2.24 eV/atom was calculated for bcc cubic Ba; these values agree reasonably well with the experimental equivalents of 5.03 Å[37] and a cohesive energy of -1.90 eV[38]. Ti has a hcp structure with calculated lattice constants of a = 2.86 Å and c = 4.54 Å (compared to experimental values of a = 2.95 and c = 4.69 Å[39]) and a total energy of -8.54 eV (compared to an experimental cohesive energy of -4.85 eV[38]).

Barium oxide (BaO) has the sodium chloride structure ($Fm\bar{3}m$, space group number 225) with a lattice constant of 5.54 Å[40] and an enthalpy of formation of -5.68 eV[41]. DFT calculations produce a lattice constant of 3.28 Å and an enthalpy of formation of -5.01 eV for BaO. Rutile TiO_2 ($P4_2/mnm$, space group number 136) has lattice constants of a = 4.59 and c = 2.96 Å[42] and an enthalpy of formation of -9.78 eV[41], in comparison to calculated values of a = 4.56 and c = 2.92 Å and an enthalpy of formation of -10.09 eV. For *h*-$BaTiO_3$ ($P6_3/mmc$, space group number 194), lattice constants of a = 5.66 and c = 13.80 Å were calculated which agree well with experimental values of a = 5.72 and c = 13.96 Å[43]. There is also excellent agreement between the calculated and experimental enthalpy of formation energies, an experimental value of 17.20 eV[44] and a calculated value of 17.19 eV. In general there is good agreement between the experimental and calculated properties of the bulk materials, however, the tendency of LDA calculations to underestimate lattice constants is clear, particularly in the cases of BaO and Ba.

B. Defect structures

All types of possible mono-vacancies were considered in *h*-$BaTiO_3$: this includes both possible sites for each vacancy and selected di-vacancies. Di-vacancies associated with the Ba2 atoms and Ti2 atoms located in the Ti_2O_9 dimers of *h*-$BaTiO_3$ were chosen because of the strong binding behaviour between these sites and oxygen vacancies and because of the preference for the formation of these defects over Ba1 and Ti1 vacancies[10], respectively. Multiple charge states were investigated for all types of vacancies. Fig. 1 shows the relaxed cell geometries for the most favourable mono-vacancies in their nominal charge state.

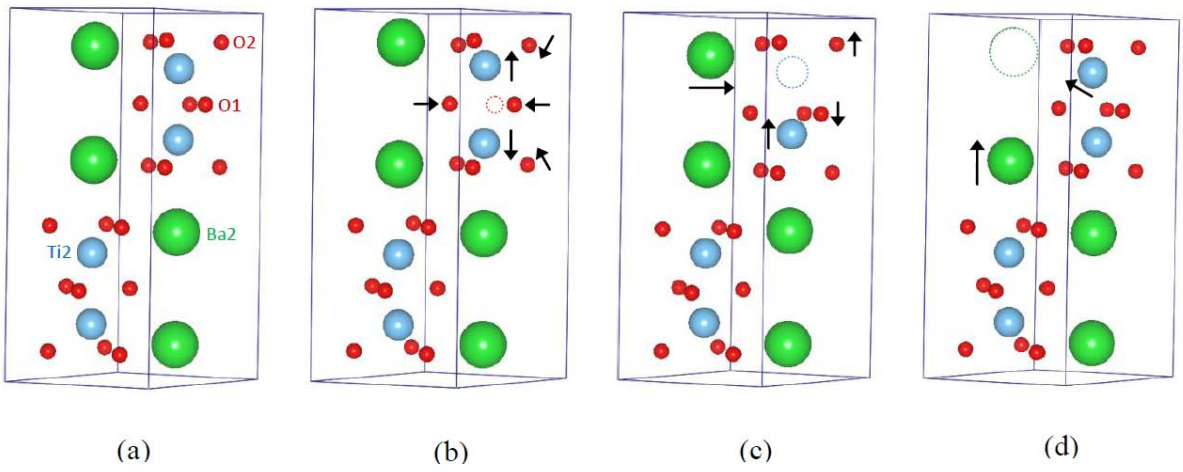

FIG. 1. (Colour online) Relaxed cell geometries for (a) - bulk *h*-$BaTiO_3$ and (b) - , (c) - , (d) - defects. Vacancy positions are shown by dashed circles and arrows denote the direction of relaxation for atoms neighbouring the vacancy. Atoms on the cell boundary (i.e. Ti1 and Ba1) and bonds have been omitted for clarity.

The introduction of a face-sharing O1 vacancy (Fig. 1(b)) to the system causes the neighbouring O1 atoms to relax inwards, while the neighbouring Ti2 atoms move away from the newly formed 2+ charged site towards the layers of O2 atoms to accommodate the loss of attraction from the loss of the O1 atom. As expected the opposite occurs for the Ti2 vacancy (Fig. 1(c)): here O1 atoms are forced away from the 4- vacancy site, whereas the surrounding Ti and Ba atoms relax towards the vacancy site. Similar relaxations were observed in DFT calculations on vacancies in anatase TiO_2[45]. For the local relaxations are not as pronounced due to the reduced charge density of a large Ba atom compared to a Ti atom. However, there is a small movement of the nearest Ba2 and Ti2 atoms towards the vacancy site (Fig. 1(d)).

C. Formation energies

The results for the calculated defect formation energies for three different combinations of chemical potentials and with a Fermi level at the valence band maximum are presented in Table I. For each vacancy type, the lowest energy vacancy (and hence most prominent) is plotted as a function of the Fermi level in Fig. 2. The values in Fig. 2 refer to a μ_O value calculated at the formation temperature of *h*-$BaTiO_3$, 1698 K, and an oxygen partial pressure of 1 atm. Only the energies of the vacancies in their nominal charge states ( ) are plotted because in the case of all vacancies, other charge states occupy a small part of the band gap or do not exist in the band gap at all.

For O vacancies, there is a clear preference for face-sharing O1 vacancies over corner-sharing O2 vacancies. This observation is confirmed by other simulations[10,11] and by experiment[9,46], where no evidence of O2 vacancies is reported for either doped or undoped *h*-$BaTiO_3$. At the

metal-rich limit, oxygen vacancies dominate over the entire band gap with negative formation energies and hence are the most abundant defect. It is noteworthy that only at the conduction band minimum (CBM) does the formation energy reach 0 eV. This suggests that under these conditions stoichiometric *h*-$BaTiO_3$ cannot form and that oxygen vacancies must always be present. This observation is confirmed by experiment, where under low (metal-rich) conditions oxygen deficient *h*-$BaTiO_3$ forms and re-oxidation is necessary to re-form the stoichiometric material[9]. The formation energies of both O1 and O2 vacancies are also considerably lower than the value found for *c*-$BaTiO_3$, where a value of -5.07 eV in metal-rich conditions was obtained[17]. This is partly supported by previous calculations, where the vacancy formation energy from lattice statics calculations for O1 in *h*-$BaTiO_3$ was lower than for an O vacancy in *c*-$BaTiO_3$, but this in turn was lower than the vacancy energy for an O2 atom[10]. The most likely reason for this discrepancy is the different approaches taken in calculating μ_O in this work and in the work by Erhart and Albe[17]. If the temperature dependence of μ_O had been taken into account in the previous work, the formation energy of an O vacancy in *c*-$BaTiO_3$ would undoubtedly have been lower. Additional error may also arise from the fact that static vacancy energy calculations do not take into account the chemical environment of the defect which makes direct comparison difficult. Under O-rich conditions, O1 vacancies only dominate in a section of the lower half of the band gap (a *p*-type material).

Unlike O vacancies, neither Ti1 nor Ti2 vacancies ever reach negative formation energies under any combination of chemical potentials at the VBM. This is to be expected because of the difficulty in removing an ion with a high charge density such as Ti^{4+} from an ionic system. In DFT calculations by Moriwake *et al.*[47] on *c*-$BaTiO_3$, Ti vacancies are not observed in any chemical environment, although this is almost certainly a result of the fact that only neutral

defects were considered. High Ti vacancy energies in both *c*- and *h*-$BaTiO_3$ have also been found using potential-based methods[10,48,49]. Regardless of this, Ti vacancies (and in particular Ti2 vacancies) dominate in O-rich conditions in the top half of the band gap (a *n*-type material). Again, good agreement is achieved with lattice statics calculations as the Ti vacancy formation energies published here are higher than those for the cubic phase[17], which is also true for the classical calculations[10]. It should be noted that Ba-site doping with trivalent lanthanides such as La in *c*-$BaTiO_3$ does produce a substantial solid solution (~25 at%) where the compensation mechanism is the formation of Ti-vacancies, i.e. $Ba_{1-x}La_xTi_{1-x/4}O_3$ with 0 0.25[50].

The results for the formation energy of Ba vacancies suggest that for the majority of the band gap it is not the dominant species, either in metal-rich or O-rich conditions (although the magnitude of the formation energies is reasonable with respect to the other vacancy types). Fig. 2 shows that for only a small portion of the band gap (E_F = ~1.6 to 2.1 eV) in O-rich (Ba deficient) conditions does the Ba2 vacancy species become the dominant defect in the material. This may seem surprising considering the energetic penalty of removing a highly charged Ti vacancy. However, unlike a , a Ba vacancy does not have such a strong dependence on the Fermi level (2- charge compared to a 4- charge), that allows Ti vacancies to dominate in the top half of the band gap. Furthermore, calculations on the cubic polymorph also showed only a small area of the band gap in a similar chemical environment where Ba vacancies are the predominant defect[17] and previous calculations suggest Ba vacancies in *h*-$BaTiO_3$ are less favourable than in *c*-$BaTiO_3$[10]. Direct comparison with experiment is difficult for $BaTiO_3$, as Ba and Ti vacancy abundances are measured in doped samples where the concentrations of such vacancies are strongly influenced by the nature of the dopant species[51].

Given the strong Coulombic interaction between point defects in $BaTiO_3$, it is necessary to consider the formation of defect pairs between negatively charged metal vacancies and positively charged oxygen vacancies. The binding energy (E_b) of such a defect pair gives an insight into whether the defects prefer to pair or remain isolated. The binding energy of a defect pair/complex is calculated by: -

(10)

where and are the formation energies of the constituents and is the formation energy of the binding pair. The binding energy is independent of chemical potentials and a negative value suggests that the defect pair will readily form. Binding energies of -0.35 eV and -0.08 eV were calculated for and , respectively. For the Ti vacancy pairs, binding energies of -0.25 eV and -1.01 eV were observed for and , respectively. This clearly suggests that defect pairs will readily form where possible, with and di-vacancies having the energetic preference, although, as previously discussed, in reality the presence of defects has not been observed experimentally. Erhart and Albe[17] obtained significantly stronger binding energies of -0.62 eV and -1.93 eV for the equivalent Ba-O and Ti-O di-vacancies in the cubic structure. The proposed reason for the greater Ti-O binding in the cubic polymorph is that for these types of di-vacancies in *h*-$BaTiO_3$, there is competition between the attraction of the negatively charged with both the positively charged and the neighbouring Ti2 atom. This scenario does not exist for *c*-$BaTiO_3$ as all Ti atoms are separated by 4.00 Å and hence the Coulombic attraction is not as strong. In the case of the di-vacancy, there is also increased strain because of the close proximity of surrounding O1 and O2 atoms which are attracted to , but experience repulsion from the

binding resulting in less favourable binding behaviour. A similar explanation can also account for the difference in the Ba-O binding energies between the two polymorphs as Ba atoms are also separated by ~4.00 Å in the cubic polymorph. As proposed in Ref. 17, it is most likely that oxygen vacancies bind to the immobile metal vacancies as they diffuse through the system.

TABLE I: Formation energies of mono- and di-vacancies in *h*-$BaTiO_3$ under metal-rich and O-rich conditions at T = 1698 K, = 1 atm and with the Fermi level at the valence band maximum (E_F = 0 in Eq. (1)). Values relevant to the band gap correction (Eq. (9)) are given in the third column. The finite-size extrapolation error is given in the final column.

Defect	q	$n_{e,h}$	E_f (eV) (Metal-rich)	E_f (eV) (O-rich)[1]	E_f (eV) (O-rich)[2]	Error (eV)
V_{O1}	0	-2	1.77	6.14	6.14	(0.19)
	+1	-1	-2.60	1.77	1.77	(0.11)
	+2	0	-6.80	-2.43	-2.43	(0.07)
V_{O2}	0	-2	2.55	6.92	6.92	(0.14)
	+1	-1	-1.82	2.55	2.55	(0.05)
	+2	0	-6.03	-1.66	-1.66	(0.12)
V_{Ba1}	-2	0	10.47	4.73	6.54	(0.20)
	-1	+1	9.82	4.08	5.89	(0.14)
	0	+2	9.22	3.48	5.29	(0.02)
V_{Ba2}	-2	0	10.21	4.47	6.28	(0.09)
	-1	+1	9.63	3.89	5.70	(0.02)
	0	+2	9.04	3.30	5.11	(0.14)
V_{Ti1}	-4	0	17.50	10.13	8.04	(0.35)
	-3	+1	17.00	9.63	7.54	(0.33)
	-2	+2	16.45	9.08	6.99	(0.23)
	-1	+3	15.92	8.55	6.46	(0.11)
	0	+4	15.37	8.00	5.91	(0.11)
V_{Ti2}	-4	0	16.25	8.88	6.79	(0.27)
	-3	+1	15.74	8.37	6.28	(0.30)
	-2	+2	15.27	7.9	5.81	(0.21)
	-1	+3	14.73	7.36	5.27	(0.08)
	0	+4	14.24	6.87	4.78	(0.09)
V_{Ba2} - V_{O1}	-1	-1	7.39	6.02	8.11	(0.17)
	0	0	3.06	1.69	3.78	(0.07)
	+1	+1	2.31	0.94	3.03	(0.09)
V_{Ba2} - V_{O2}	-1	-1	8.39	7.02	9.11	(0.23)
	0	0	4.10	2.73	4.82	(0.14)
	+1	+1	3.49	2.12	4.21	(0.13)
V_{Ti2} - V_{O1}	-3	-1	13.37	10.37	8.28	(0.12)
	-2	0	9.20	6.20	4.11	(0.16)
	-1	+1	8.62	5.62	3.53	(0.08)
	0	+2	8.03	5.03	2.94	(0.06)
	+1	+3	7.44	4.44	2.35	(0.17)
V_{Ti2} - V_{O2}	-3	-1	13.32	10.32	8.23	(0.22)
	-2	0	9.21	6.21	4.12	(0.31)

-1	+1	8.45	5.45	3.36	(0.24)
0	+2	7.83	4.83	2.74	(0.07)
+1	+3	7.21	4.21	2.12	(0.09)

[1]O-rich environment where is at the maximum negative value defined by Eqs. 4 and 5.
[2]O-rich environment where is at the maximum negative value defined by Eqs. 4 and 5.

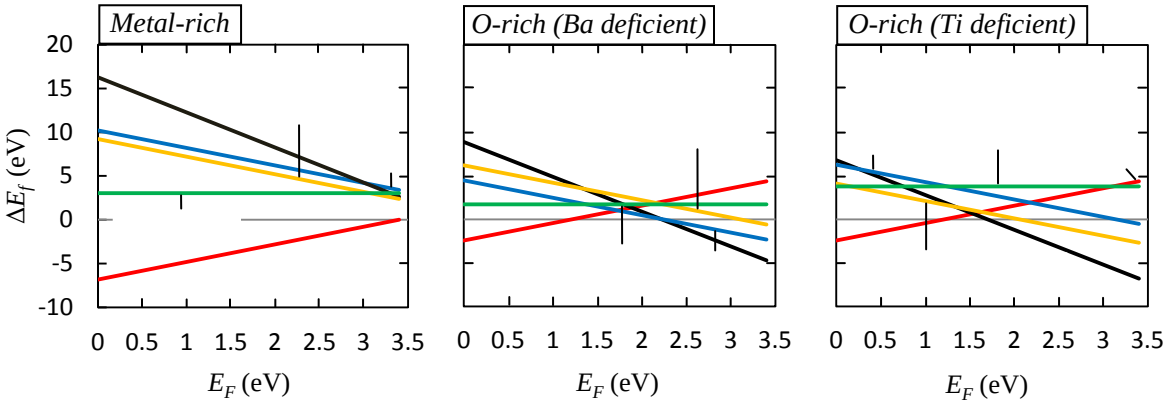

FIG. 2. (Colour online) Variation of calculated defect formation energies of the lowest energy vacancy types in *h*-$BaTiO_3$ with Fermi level energy (E_F). Formation energies refer to the defect in its nominal charge state. The calculation of μ_O was performed at T = 1698 K and = 1 atm.

D. Defect concentrations

Using the calculated defect formation energies at a specific combination of chemical potentials, the equilibrium defect concentrations can be calculated using Eq. 2. The concentrations of the most common defects at a range of temperatures in both Ba- and Ti-deficient environments are given in Fig. 3. The concentrations are calculated at the Fermi level pinning energy (1.22 eV), this value represents the point at which the Fermi level of the material

cannot be closer to the valence band as the formation energy of certain defects becomes negative meaning that the stoichiometric material is not stable. Metal-rich conditions are not considered as the high formation energies of metal vacancies in this environment means that the concentrations will be negligible for most values of the Fermi energy. O vacancies are also omitted, as at the Fermi level pinning energy their formation energies are very low and will hence be very high in concentration and will always be the dominant defect.

At the pinning energy and under Ba-deficient conditions, titanium mono- and di-vacancies are low in concentration, with di-vacancies being preferred (~7.0 x 10^{10} cm^{-3} for V_{Ti2} - V_{O1} at 1698 K compared to ~1.3 x 10^{10} cm^{-3} for V_{Ti2} at the same temperature). Conversely, barium mono- and di-vacancies are significantly higher in concentration. V_{Ba2} - V_{O1} shows the highest concentration for metal vacancies in Ba-deficient conditions with a concentration of ~9.7 x 10^{16} cm^{-3} at 1698 K, an order of magnitude more than the second most important defect, V_{Ba2}. These vacancy concentrations are only valid for the undoped material as cation vacancies are often involved in compensating donor doped systems and will hence exist in higher concentrations in such doped systems[52,53].

In Ti-deficient conditions, the V_{Ti2} - V_{O1} di-vacancy pair is the commonest metal defect in the system. The concentration of these di-vacancies proves that where possible metal vacancies will preferentially bind to oxygen vacancies to lower the internal energy of the crystal. This is also confirmed by a molecular dynamics study on doped $BaTiO_3$, where diffusion of V_O is inhibited by its Coulombic attraction to cation vacancies[54]. Mono-titanium vacancies are also present in significant concentrations, while other defects are only present in far smaller concentrations.

These results have been confirmed by experiment and thermodynamics calculations for both the cubic and hexagonal polymorphs of $BaTiO_3$[55,56]. Lee *et al*[55] showed using XRD and by studying the phase transition temperature variation with respect to the Ba/Ti ratio that a greater solubility limit exists under Ba-rich (Ti-deficient) conditions than previously thought in addition to the already known solubility limit of the Ti-rich (Ba-deficient) side. This solubility in both Ba- and Ti-rich conditions suggests that both Ba and Ti metal vacancies are likely and that they will exist as partial-Schottky defects (V_{Ba} - V_O and V_{Ti} - $2V_O$) in the system, a finding confirmed by thermodynamic theory[56].

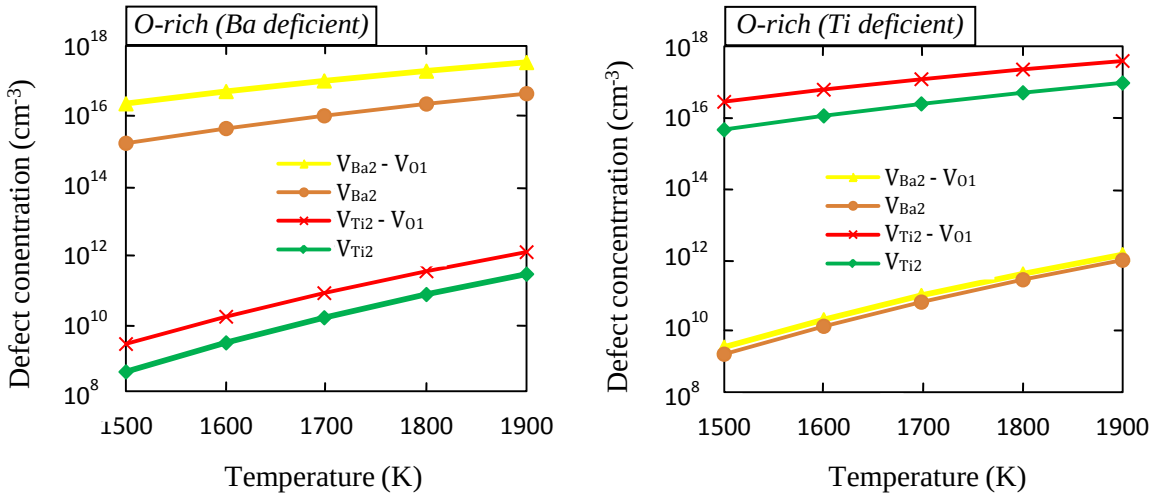

FIG. 3. (Colour online) Defect concentrations of V_{Ti2}, V_{Ba2}, V_{Ti2} - V_{O1} and V_{Ba2} - V_{O1} in their nominal charge states for temperatures in the range 1500 – 1900 K at the Fermi level pinning energy (1.22 eV) in *h*-$BaTiO_3$.

IV. CONCLUSIONS

In this work, we have completed an extensive density functional theory study of the intrinsic defects in *h*-$BaTiO_3$. All possible mono-vacancies have been considered as well as metal-oxygen di-vacancies and all vacancies have been considered in a range of possible charge states. Defect formation energies have been calculated using the Zhang-Northrup formalism[20] with necessary consideration given to the errors arising from the supercell approach and from the error associated with the calculation of the band-gap in DFT studies. The method of Finnis, Lozovoi and Alavi[21] has also been applied for the calculation of the oxygen chemical potential to limit inaccuracies arising from the direct calculation of the oxygen dimer. Equilibrium defect concentrations are derived from formation energies for a range of temperatures.

Calculations confirmed that all types of vacancies studied exist in their nominal charge state over the majority of the band gap and that generally V_{O1} is the dominant defect in the system in accordance with experiment. Under metal-rich conditions, the formation energy of V_{O1} remains negative for all values of the Fermi level up to the conduction band minimum. This suggests that under such a low oxygen partial pressure, stoichiometry cannot exist in the system, a finding supported by experiment[9]. For oxygen-rich conditions, V_{O1} again dominates in the lower half of the band gap, while in the upper half metal di-vacancies are the most prevalent defects. Binding energies calculated for the V_{Ba} - V_O and V_{Ti} - V_O pairs suggest that these di-vacancies will readily form by the 'capture' of a mobile oxygen vacancy by a metal vacancy. Mono-metal vacancy concentrations are exceeded by di-vacancies concentrations, with the highest concentrated defects being V_{Ba2} - V_{O1} (~9.7 x 10^{16} cm^{-3} (1698 K)) for a Ba-deficient environment

and V_{Ti2} - V_{O1} (~1.1 x 10^{17} cm^{-3} (1698 K) for a Ti-deficient environment, as supported by experiment. Excellent agreement has also been observed with previous lattice statics and DFT calculations on the cubic polymorph of $BaTiO_3$.

ACKNOWLEDGMENTS

The authors would like Dr. P. Erhart for useful discussions regarding this publication and the UK Engineering and Science Research Council (EPSRC) for funding (Grant number – EP/G005001/1).

REFERENCES

[1]R. E. Cohen, Nature **358**, 136 (1992).

[2]S. Roberts, Phys. Rev. **71**, 890 (1947).

[3]A. Moulson and J. Herbert, *Electroceramics – Materials, Properties, Applications* (John Wiley and Sons, New York, 2003).

[4]M. Yamaguchi, K. Inoue, T. Yagi and Y. Akishige, Phys. Rev. Lett. **74**, 2126 (1995).

[5]M. Yamaguchi, M. Watanabe, K. Inoue, Y. Akishige, and T. Yagi, Phys. Rev. Lett. **75**, 1399 (1995).

[6]K. Inoue, A. Hasegawa and K. Watanabe, H. Yamaguchi, H. Uwe and T. Sakudo, Phys. Rev. B **38**, 6532 (1988).

[7]A. Feteira, K. Sarma, N. Mc. Alford, I. M. Reaney and D. C. Sinclair, J. Am. Ceram. Soc., **86**, 511 (2003).

[8]J. Yu, T. Ishikawa, Y. Arai, S. Yoda, M. Itoh and Y. Saita, Appl. Phys. Lett. **87**, 252904 (2005).

[9]D. C. Sinclair, J. M. S. Skakle, F. D. Morrison, R. I. Smith and T. P. Beales, J. Mater. Chem. **6**, 1327 (1999).

[10]J. A. Dawson, C. L. Freeman, L.-B. Ben, J. H. Harding and D. C. Sinclair, J. Appl. Phys. **109**, 084102 (2011).

[11]T. A. Colson, M. J. S. Spencer and I. Yarovsky, Comp. Mater. Sci. **34**, 157 (2005).

[12]H. Natsui, J. Yu, S. Hashimoto, M. Itoh, O. Odawara and S. Yoda, Ferroelectrics **415**, 122 (2011).

[13]H. Natsui, J. Yu, S. Hashimoto, M. Itoh, O. Odawara and S. Yoda, Ferroelectrics **403**, 225 (2010).

[14]N. Maso, H. Beltran, E. Cordoncillo, P. Escribano and A. R. West, J. Mater. Chem. **16**, 1626 (2006).

[15]H.–J. Hagemann and H. Ihrig, Phys. Rev. B, **20**, 3871 (1979).

[16]Z.-X. Chen, Y. Chen and Y.-S. Jiang, J. Phys. Chem. B. **105**, 5766 (2001).

[17]P. Erhart and K. Albe, J. Appl. Phys. **102**, 084111 (2007).

[18]P. Ghosez, J.-P. Michenaud and X. Gonze, Phys. Rev. B. **58**, 6224 (1998).

[19]E. Bousquet and P.Ghosez, Phys. Rev. B. **74**, 180101 (2006).

[20]S. B. Zhang and J. E. Northrup, Phys. Rev. Lett. **67**, 2339 (1991).

[21]M. W. Finnis, A. Y. Lozovoi and A. Alavi, Annu. Rev. Mater. Res. **35**, 167 (2005).

[22]N. D. M. Hine, K. Frensch, W. M. C. Foulkes and M. W. Finnis, Phys. Rev. B **79**, 024112 (2009).

[23]G. Kresse and J. Furthmüller, Comput. Mater. Sci. **6**, 15 (1996).

[24]D. M. Ceperley and B. J. Alder, Phys. Rev. Lett. **45**, 566 (1980).

[25]J. P. Perdew and A. Zunger, Phys. Rev. B **23**, 5048 (1981).

[26]P. E. Blöchl, Phys. Rev. B **50**, 17953 (1994).

[27]G. Kresse and D. Joubert, Phys. Rev. B **59**, 1758 (1999).

[28]A. R. Allnatt and A. B. Lidiard, *Atomic Transport in Solids* (Cambridge University Press, Cambridge, 2003).

[29]K. Johnston, M. R. Castell, A. T. Paxton and M. W. Finnis, Phys. Rev. B **70**, 085415 (2004).

[30]Condensed Phase Thermochemistry Data, NIST Chemistry WebBook, NIST Standard Reference Database Number 69, 2005, (http://webbook.nist.gov).

[31]Y.-J. Zhao, C. Persson, S. Lany and A. Zunger, Appl. Phys. Lett. **85**, 5860 (2004).

[32]D. Aberg, P. Erhart, A. J. Williamson and V. Lordi, Phys. Rev. B **77**, 165206 (2008).

[33]G. Makov and M. C. Payne, Phys. Rev. B **51**, 4014 (1995).

[34]E. Cockayne, J. Eur. Ceram. Soc. **23**, 2375 (2003).

[35]P. A. Schultz, Phys. Rev. Lett **96**, 246401 (2006).

[36]S. H. Wemple, Phys. Rev. B **2**, 2679 (1970).

[37]J. Evers**,** G. Oehlinger**,** B. Sendlinger**,** A. Weiss, M. Schmidt and P. Schramel**,** J. Alloy Comp. **182**, 175 (1992).

[38]C. Kittel, *Introduction to Solid State Physics*, 8th ed. (Wiley, New York, 2004).

[39]R. R. Pawar and V. T. Deshpande, Acta Crystallogr. **24A**, 316 (1968).

[40]R. J. Zollweg, Phys. Rev. **100**, 671 (1955).

[41]D. Lide, *CRC Handbook of Chemistry and Physics*, 68th ed. (CRC Press, Boca Raton, 1998).

[42]S. C. Abrahams and J. L. Bernstein, J. Chem. Phys. **55**, 3206 (1971).

[43]H. Arend and L. Kihlborg, J. Am. Ceram. Soc. **52**, 63 (1969).

[44]M. Karapet'yants and M. Karapet'yants, *Handbook of Thermodynamic Constants of Inorganic and Organic Compounds*, 68th ed. (Ann Arbor – Humphrey Science Publishers Inc, Ann Arbor, trans J. Schmorak, 1970).

[45]S. Na-Phattalung, M. F. Smith, K. Kim, M.-H. Du, S.-H. Wei, S. B. Zhang and S. Limpijumnong, Phys. Rev. B **73**, 125205 (2006).

[46]A. Feteira, G. M. Keith, M. J. Rampling, C. A. Kirk, I. M. Reaney, K. Sarma, N. Mc. Alford and D. C. Sinclair, Cryst. Eng. **5**, 439 (2002).

[47]H. Moriwake, Int. J. Quantum Chem. **99**, 824 (2004).

[48]C. L. Freeman, J. A. Dawson, H.-R. Chen, J. H. Harding, L.-B. Ben and D. C. Sinclair, J. Mater. Chem. **21**, 4861 (2011).

[49]M. T. Buscaglia, V. Buscaglia, M. Viviani and P. Nanni, J. Am. Ceram. Soc. **84**, 376 (2001).

[50]F. D. Morrison, D. C. Sinclair and A. R. West, J. Appl. Phys., **86**, 6355 (1999).

[51]T. D. Dunbar, W. L. Warren, B. A. Tuttle, C. A. Randall and Y. Tsur, J. Phys. Chem. B **108**, 908 (2004).

[52]N.-H. Chan and D. M. Smyth, J. Am. Ceram. Soc. **67**, 285 (1984).

[53]A. Yamada and Y.-M. Chiang, J. Am. Ceram. Soc. **78**, 909 (1995).

[54]T. Oyama, N. Wada and Y. Sakabe, Key Eng. Mater. **388**, 269 (2009).

[55]S. Lee, C. Randall and Z.-K. Liu, J. Am. Ceram. Soc. **90**, 2589 (2007).

[56]S. Lee, C. Randall and Z.-K. Liu, J. Am. Ceram. Soc. **91**, 1748 (2008).